Fuel 364 (2024) 130994

Contents lists available at ScienceDirect

Fuel

journal homepage: www.elsevier.com/locate/fuel

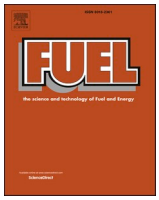

Full Length Article

Improving process sustainability in bio-oil transforming for biofuels and platform chemicals production: Valorization of the carbon residue

Beatriz Valle [a,*], Eriz Corro [b], Roberto Palos [a], Iratxe Crespo [a], M. Mirari Antxustegi [b], Pedram Fatehi [c], María González-Alriols [b]

[a] Department of Chemical Engineering, University of the Basque Country UPV/EHU, P.O. Box 644, Bilbao 48080, Spain
[b] Biorefinery Processes Research Group (BioRP), Chemical and Environmental Engineering Department, University of the Basque Country UPV/EHU, Av. Otaola 29, Eibar 20600, Spain
[c] Chemical Engineering Department and Biorefining Research Institute, Lakehead University, Thunder Bay, ON P7B5E1, Canada

ARTICLE INFO

Keywords:
Bio-oil valorization
Carbon residue
Activated carbon
Wastewater treatment

ABSTRACT

This work introduces a zero-waste approach to process biomass-derived raw bio-oil by addressing the valorization of the carbon residue that inevitably deposits, reducing the bio-oil conversion efficiency and leading to reactor-clogging issues. The study explores the feasibility of producing value-added porous material for removing pollutants from industrial wastewaters. An activated carbon with a specific surface area of 1070 $m^2\ g^{-1}$ and a micropore volume of 0.41 mL g^{-1} was successfully produced through a simple thermochemical method involving pyrolysis, alkaline treatment, and carbonization. The impact that the activation method has on the nature, structure, and adsorption capacity of the material was assessed using methylene blue (MB) and hexavalent chromium (Cr-VI) as probe molecules. The activated carbon exhibited remarkable adsorption efficiency, achieving a removal ratio of 98 % for MB and 47 % for Cr-VI. Recyclability tests demonstrated a slight loss of adsorption capacity over multiple cycles. Kinetic studies, employing Surface Reaction Models and Mass Transfer Modeling, provide insights into adsorption rate-limiting steps. Chemisorption was identified as the most limiting stage, with physisorption and liquid film diffusion playing roles, particularly at short solid–liquid contact times. For longer contact times, intraparticle pore diffusion becomes the rate-controlling step due to the highly microporous nature of the activated carbon.

1. Introduction

As the world seeks to transition towards a sustainable energy model, the demand for alternative and eco-friendly sources of fuels and petrochemicals has become increasingly urgent. In this context, lignocellulosic biomass, a renewable resource that is widely available, has attracted growing attention due to its carbon–neutral lifecycle [1]. One of the most promising valorization routes for this biomass is fast pyrolysis, which has reached high technological development in recent decades, thanks to the potential applications of the liquid product (bio-oil) [2,3]. This bio-oil consists of water (21–23 wt%) and a wide range of oxygen-containing organic compounds, from small molecules like alcohols, phenols, and carboxylic acids to high-molecular weight sugar-derived oligomers and phenolic compounds [4,5]. This composition renders bio-oil an attractive source for producing biofuels, hydrogen, and other platform chemicals [6,7]. However, the commercialization of raw bio-oil valorization processes is still in its early stages due to technical and economic constraints. Hence, further techno-economic research is necessary to identify the bottlenecks in these processes.

Traditionally, the deposition of carbon material during bio-oil processing has been considered as a hindrance, causing blockage issues in reactor and catalyst deactivation [8]. The formation of thermal-origin carbon is related to the presence of thermally unstable oxygenates prone to polymerization (mainly phenolic oligomers), while catalyst deactivation is attributed to the condensation of polycyclic aromatics [9–12]. Several physical treatments have been addressed to overcome these issues, including addition of stabilizers (alcohols) and thermal or pressure pre-treatments. By employing a two-step (thermal-catalytic) strategy, originally proposed by Gayubo et al. [13], we have successfully controlled the thermal deposition of carbon residue from bio-oil, thereby enhancing the subsequent catalytic valorization into hydrogen (via steam reforming [14–16]) and hydrocarbons (via catalytic

* Corresponding author.
E-mail address: beatriz.valle@ehu.es (B. Valle).

https://doi.org/10.1016/j.fuel.2024.130994
Received 13 November 2023; Received in revised form 28 December 2023; Accepted 13 January 2024
Available online 1 February 2024

cracking) [13,17]. However, the thermal processing of raw bio-oil still results in a substantial quantity of carbon residue.

In this study, we introduce a pioneering approach to address the production of value-added porous materials from this residue. While the valorization of bio-oil has been a focus of research, the effective valorization of the resulting carbon residue has been little explored in the literature and would represent a significant advancement to increase the carbon efficiency of bio-oil valorization, improving process sustainability and economic throughput [18]. This work explores the synthesis of activated carbon and its application in pollutant removal. To the best of our knowledge, this is the first comprehensive investigation into the detailed utilization of this residue as activated carbon, highlighting its potential in wastewater treatment. This area is increasingly important due to growing concerns about industrial pollutant discharge.

Biosorption has several advantages over traditional physicochemical methods (e.g., membrane filtration, coagulation, ion exchange, chemical precipitation) in terms of low cost, high efficiency, and the ability to target specific pollutants [19,20]. Many studies have shown the potential and attributes of biochar produced from various biomass wastes as effective adsorbents for removing contaminants from wastewater [21–23]. Activation methods can be employed to enhance the properties of bio-derived carbons, thereby addressing their limitations such as slow diffusion, low stability, and variable performance [24–26]. The ongoing progress in bio-derived carbon production and application highlights its potential for the development of cost-effective and sustainable adsorbents with high efficiency in removing pollutants, which is critical for successful wastewater treatment. Conducting systematic studies is necessary to gain knowledge on emerging trends and the direction of research.

Several crucial aspects that determine the effectiveness of an adsorbent for wastewater decontamination have been assessed in this work. To analyze the versatility of the synthesized carbon, two types of pollutants were chosen as probe molecules due to their diverse physicochemical properties and environmental relevance: methylene blue and hexavalent chromium. Methylene blue is a cationic dye widely used in several industries, such as wood, paper, and leather processing. Dyeing wastewater accounts for a significant portion of the total industrial wastewater. In the textile sector, 200 billion liters of pigments are produced annually, with up to 50 % of the effluents being discharged into aquatic systems [27,28]. Due to its well-defined structure, methylene blue is a widely used molecule to simulate the adsorption of organic pollutants. Its application in adsorption studies is well-documented in the literature, providing a reliable reference for evaluating the efficacy of adsorbents [29,30].

On the other hand, hexavalent chromium is a notorious heavy metal contaminant known for its high toxicity and environmental persistence. The development of effective adsorbents for its removal is gaining importance due to the presence of this metal in numerous industrial effluents, including those from tanning, painting, metal coating, and metallurgy [31,32].

The adsorption mechanisms of methylene blue and hexavalent chromium differ significantly due to their different chemical properties and interactions with adsorbents. Methylene blue, as a cationic dye, typically undergoes electrostatic interactions and hydrogen bonding with the surface functional groups of activated carbons. This is primarily attributed to the positively charged nature of methylene blue molecules [33]. Conversely, the adsorption mechanism of hexavalent chromium may encompass various chemical interactions, including reduction, co-precipitation, and ion exchange with functional groups on the activated carbon surface. Reduction of Cr(VI) to less toxic Cr(III) may also take place, leading to the formation of stable complexes or precipitates on the activated carbon surface [34].

The different adsorption mechanisms of these probe molecules may lead to differences in their affinity for the carbon surface, influencing the overall adsorption efficiency. This study aims to provide comprehensive insights into the behavior of bio-oil derived carbon for the adsorption of both organic and inorganic pollutants.

The regeneration potential of the synthesized activated carbon has also been evaluated. The regeneration of an adsorbent after reaching the saturation point is crucial so that the material can be used in multiple adsorption–desorption cycles. It reduces the demand for fresh adsorbent and minimizes the waste of spent adsorbent, enhancing its reusability. This, in turn, helps to minimize operational costs and to reduce the environmental impact associated with the accumulation of spent adsorbent. Developing a simple, efficient, and cost-effective recovery process could generate greater interest in producing bio-based adsorbents for wastewater treatment.

Finally, a comprehensive understanding of the adsorption mechanism of methylene blue onto the activated carbon has been achieved through an investigation on the adsorption kinetics. Gaining knowledge of the kinetic model offers valuable insights into the fundamental phenomena involved in the adsorption process, including surface reactions, external/liquid film diffusion, intraparticle pore diffusion and intrinsic adsorption reactions [35,36]. In addition, studying adsorption kinetics helps to predict the performance of the adsorbent and to identify the breakthrough point (saturation) under varying conditions. Determining the adsorbent lifespan and knowing when it requires replacement or regeneration is crucial for optimizing the design and operation of adsorption systems. Consequently, investigating the adsorption kinetics of pollutants is essential for the development of effective methods to remove pollutants from wastewater.

2. Materials and methods

2.1. Production of carbon material from bio-oil

The bio-oil was produced by fast pyrolysis of pine sawdust and provided by BTG Bioliquids (The Netherlands). Further details on the production process and composition of this bio-oil are provided in the Supporting Information.

The carbon residue used in this study, named Raw-BC, is obtained from a two-step reaction setup. In the thermal unit of this system, the raw bio-oil is introduced as droplets through an inert N_2 flow (Fig. 1). The controlled deposition of carbon material in this thermal step is a key strategy to enhance the subsequent catalytic valorization of bio-oil oxygenates. Generally, deposition decreases as the unit temperature is increased (ranging from 21 wt% at 400 °C to 2 wt% at 700 °C). An optimal temperature of 500 °C was determined for achieving a suitable composition of bio-oil oxygenates stream for the subsequent catalytic step. At this temperature, approximately 13–15 wt% of the raw bio-oil fed is deposited as carbon residue (Raw-BC), while 8 wt% is decomposed into gases (CO, CO_2, CH_4). For more information on the collection process, including factors influencing carbon residue yield and composition, such as bio-oil characteristics and operating temperature, refer to the Supporting Information.

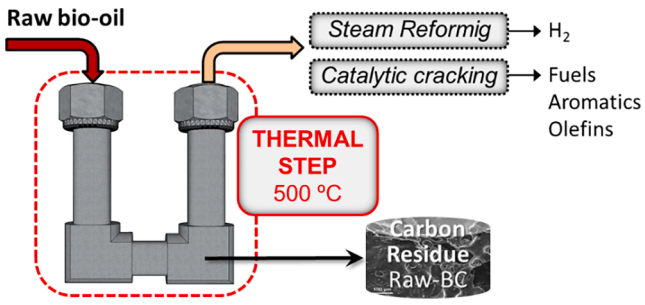

Fig. 1. Production of carbon material from raw bio-oil in the two-step (thermal-catalytic) reaction system.

2.2. Activation of bio-oil derived carbon material

To produce the activated carbon (Act-BC), the Raw-BC was subjected to a procedure previously established as suitable for obtaining activated biochar from lignocellulosic biomass samples. This process involves a pyrolysis treatment followed by chemical activation [37].

The pyrolysis stage was carried out using a horizontal tube furnace, *Carbolite GHA & GHC* model, with a heating rate of 10 °C min^{-1} up to 900 °C and maintaining this temperature for 1 h under an inert atmosphere (40 L min^{-1} N_2 flow). After completion of this process, the sample was gradually cooled down to room temperature inside the furnace while maintaining the N_2 flow. The resulting pyrolysis-treated sample, referred to as Pyr-BC, was subsequently subjected to chemical activation by being mechanically mixed with KOH in a 1/1 mass ratio. This mixture was then carbonized in the same furnace at a heating rate of 20 °C min^{-1}, reaching 900 °C, and maintained at that temperature for 2 h with a 20 L min^{-1} N_2 flow. Afterwards, the sample was cooled down to room temperature under a N_2 atmosphere. Following the activation process, the sample underwent a thorough washing procedure consisting of three steps: i) washing with deionized water; ii) washing with a 3.8 M HNO_3 solution; and iii) another round of washing with deionized water until achieving a neutral pH. Finally, the sample was dried at 105 °C for 12 h.

2.3. Characterization of carbon materials

Elemental, proximate, and thermogravimetric analyses were initially conducted on the Raw-BC material to gather essential information on its characteristics and composition. This information was crucial for establishing appropriate conditions for the activation treatment. The sample's carbon, hydrogen, nitrogen, and sulfur contents were quantified using a *TruSpec Micro LECO* elemental analyzer (CHNS). The measurements of volatile matter, ash content, moisture, and calorific value were carried out using an *IKA C200 Calorimeter* device (following standards for volatile matter UNE-EN 15148–2010, mineral matter UNE-EN 14,775 and moisture UNE-EN 14774-3).

Thermogravimetric analysis was conducted using a *TA Instruments Q5000* thermobalance to investigate the carbonization properties of the Raw-BC carbon precursor. The sample underwent heating from 25 to 900 °C at a heating rate of 5 °C min^{-1} under an inert atmosphere (N_2 flow of 50 mL min^{-1}), and it was maintained at 900 °C for 20 min. Throughout the heating process, the mass of the sample was continuously monitored and recorded in real-time.

The features of the functional groups located on the surface of each carbon material were analyzed using Fourier-transform infrared spectroscopy (FTIR) employing a *Nicolet 6700 Thermo Fisher Scientific* device. To prepare solid pellets for analysis, each sample was compressed at 10 tons for 15 min together with KBr (10 wt%). The scanning was performed at 25 °C, following a drying step (heating up to 150 °C) to prevent moisture interference during measurement. The spectra were collected within the 3800–600 cm^{-1} range with a resolution of 4 cm^{-1} and 100 scans per spectrum.

The microscopic structure and morphology of the raw carbon material (Raw-BC) as well as the prepared carbons Pyr-BC and Act-BC were examined by Scanning Electron Microscopy (SEM) using a *JEOL JSM-7000F* microscope. Observations were made at various magnifications (500x, 3kx, and 10kx).

The specific surface area and pore structure of Act-BC sample were analyzed by gas (N_2 and CO_2) physisorption experiments. N_2 adsorption/desorption isotherms were obtained at −196 °C using an *ASAP 2010 Micromeritics* analyzer, following overnight outgassing under vacuum at 150 °C. The specific surface area was determined using the Brunauer-Emmet-Teller (BET) method, the micropore volume was calculated using the *t*-plot method based on the Harkins-Jura equation, and the pore size distribution was calculated applying non-local density functional theory (NLDFT). To address diffusion issues related to N_2 and evaluate narrow microporosity, the textural properties of the Pyr-BC sample were determined by CO_2 physisorption measurements. Adsorption/desorption isotherms were collected at 0 °C using an *ASiQwin Quantachrome* device after overnight outgassing of the sample under vacuum at 150 °C. The surface area, micropore volume, and average pore width were quantified by applying the NLDFT theory.

2.4. Adsorption effectiveness of synthesized activated carbon

The adsorption effectiveness of Act-BC was assessed through batch experiments. In these experiments, 0.15 g of Act-BC were added to 25 mL of a solution containing either methylene blue (MB) or hexavalent chromium (Cr(VI)). The initial concentrations of the MB and Cr(VI) solutions were 35 mg L^{-1} and 100 mg L^{-1}, respectively. The adsorption capacity of Act-BC was compared with that of the raw material (Raw-BC) and the pyrolysis-treated sample (Pyr-BC), enabling the evaluation of the impact of activation process on the adsorption capacity.

The adsorption experiments were carried out at 25 °C for various durations (1, 2, 4, 8, and 24 h). To ensure optimal interaction between the adsorbent and pollutant, the solid–liquid mixture was stirred for 5 min. At the end of each specified time, the mixture was filtered, and the concentration of the remaining pollutant in the filtrate was determined using direct UV–VIS spectrometry. The absorbance values of the collected aliquots were measured employing a *Jasco UV–VIS V-750ST* spectrophotometer. For samples containing MB pollutant, the wavelength used was 665 nm, whereas for samples with Cr(VI) pollutant (after adjusting the pH to the 4–5 range), the wavelength was set at 350 nm.

Direct UV–VIS spectrometry is a better method for measuring Cr(VI) concentration compared to the commonly used 1,5-diphenylcarbazida colorimetry (DPC) [38]. The DPC method has limitations, as it can only be used for low concentrations and has stability issues with the produced complex. In contrast, direct UV–VIS can measure a wide range of concentrations, including levels required by EU regulations and high concentrations in industrial wastewater [39]. This method is faster and more reliable, eliminating complex preparation steps, making it an efficient way to measure Cr(VI) concentration.

The adsorption effectiveness of each carbon material was assessed by determining the adsorption capacity Q_e , Eq. (1), which quantifies the amount of pollutant that can be adsorbed by the material, and the removal ratio R, Eq. (2), which measures the efficiency of the adsorption by expressing the percentage of the pollutant removed from the solution.

$$\text{Adsorption capacity} \Rightarrow \quad Q_e = \frac{C_0 - C_e}{m_{BC}} \cdot V \tag{1}$$

$$\text{Removal ratio} \Rightarrow \quad R = \frac{C_0 - C_e}{C_0} \cdot 100 \tag{2}$$

where V is the volume of solution (L), C_0 is the pollutant solution concentration (mg L^{-1}), C_e refers to the concentration of solution at equilibrium (mg L^{-1}), and m_{BC} is the mass of the carbon material (g).

2.5. Recyclability of synthesized activated carbon

The regeneration and reuse capacity of Act-BC was assessed for the adsorption of methylene blue (MB). The desorption of Cr(VI) involves surface complexation phenomena, so further research is needed to design an effective regeneration process for its removal.

The regeneration process involves the desorption of MB from the adsorbent, typically using two types of methods: i) degradation, which involves the decomposition of adsorbed MB using techniques such as thermal degradation, microwave irradiation, or photodegradation; and ii) physical desorption, which has been widely investigated to regenerate carbon adsorbents and to recover the MB [29].

For the recyclability study, the behavior of the material has been

examined in four consecutive adsorption–desorption cycles. The spent Act-BC adsorbent, after being separated from the MB solution through filtration, was dried at 60 °C for 24 h. Subsequently, the dried spent adsorbent was placed in a flask containing pure acetone, chosen as the regeneration solvent due to its low boiling point and proven efficacy from previous research [40]. To ensure optimal liquid–solid contact, the mixture was stirred for the initial 5 min and then left in contact with acetone for up to 3 h. This limited stirring duration aimed to minimize sample loss. After the regeneration process, the adsorbent was filtered, washed with distilled water, and dried again at 60 °C for 24 h. The desorption methodology selected for this study was based on its simplicity and low cost. Developing a recovery process that is simple, efficient, and cost-effective could generate increased interest in our bio-based adsorbent.

In order to address issues related to sample loss during the regeneration stages of filtration, washing and drying, the recovered adsorbent was weighted before each adsorption cycle. This practice allowed for the adjustment of the volume of MB solution, ensuring it was reduced as necessary to maintain a consistent adsorbent/pollutant ratio throughout the recyclability study.

2.6. Adsorption kinetics of synthesized activated carbon

To conduct the kinetic study, pollutant removal experiments were performed with the analysis of adsorption parameters in a continuous mode. This method offers advantages over the batch adsorption process because it provides more data in less time and avoids potential disturbances that could affect the results, such as induced agitation during aliquot collection and loss of material during filtration. By employing this approach, a more comprehensive and accurate transient concentration profile can be obtained.

In this study, a solid–liquid mixture was prepared in a UV–VIS spectroscopy quartz cuvette, with a dosage of 6 g L^{-1} of Act-BC and 35 mg L^{-1} of methylene blue (MB) as the pollutant. After an initial stirring and 10 s of ultrasound activity to ensure the proper dispersion of particles and optimal solid–liquid contact, the quartz cuvette was placed in a *Jasco UV–VIS V-750ST* spectrophotometer. In order to generate sufficient adsorption data for the kinetic study, this experiment was conducted in long-duration mode, lasting 51 h with absorbance values recorded every 30 s.

3. Results and discussion

3.1. Characteristics of raw carbon material (Raw-BC)

The elemental and proximate analyses of the bio-oil derived carbon sample (Raw-BC) are detailed in Table 1. The elemental composition demonstrates that carbon and oxygen constitute the major components of this material (approximately 95 wt%), with a minor proportion of hydrogen (4 wt%), and trace amounts of sulfur and nitrogen. Proximate analysis reveals that Raw-BC is predominantly composed of fixed carbon (≈ 60 wt%) and volatile matter (≈ 37 wt%). The low ash content (0.2 wt %) can be attributed to the retention of inorganic compounds from lignocellulosic biomass in the solid produced during the fast pyrolysis (char), resulting in minimal inorganic material in the liquid product (bio-oil).

Table 1
Elemental and proximate analysis of raw carbon material (Raw-BC).

Elemental composition (wt% dry basis)	
C	79.7
H	4.0
N	0.7
S	0.4
O*	15.2
Proximate analysis (wt% dry basis)	
Moisture	2.5
Volatiles	37.4
Ash	0.3
Fixed carbon	59.8
Calorific value (MJ kg^{-1})	17.1

* Calculated by difference (ash removed)

Due to its low calorific value (17.1 MJ kg^{-1}) in comparison with conventional fuels such as gasoline (42–46 MJ kg^{-1}) and diesel (42–45 MJ kg^{-1}) [41], along with its low H/C ratio (0.05), there is a growing preference to prioritize the valorization of Raw-BC for the production of activated carbons instead of using it as an energy source [42].

Thermogravimetric analysis (TG) was performed to investigate the thermal decomposition (carbonization) mechanism of the raw carbon material. The derivative weight loss (DTG) profile of Raw-BC (Fig. 2) shows a weight loss of approximately 1 wt% below 150 °C, attributing to moisture evaporation. The weight loss within the 150–250 °C range remains relatively low. Thermal degradation begins around 250 °C, characterized by an initial rapid stage (250–550 °C) where the rate of weight loss peaks (0.78 wt% min^{-1} at 420 °C), followed by a slower degradation stage (above 550 °C). The volatile matter removed in each stage accounts for 22 % and 12 % of the initial weight of Raw-BC, respectively.

The carbonization profile shown in Fig. 2 corresponds to the three-step thermal degradation observed in various lignin species, including Kraft, Klason and alkaline lignin [43,44], confirming the lignin-like characteristics of this material. Because of its high carbon content (as indicated in Table 1), only about 35 % of the initial material is lost during carbonization. This fact is in contrast to the higher losses reported for biomass feedstock, which can reach up to 80 % [45].

3.2. Effect of activation on the nature and morphology of carbon materials

3.2.1. Surface functional groups

The FTIR absorbance results, depicted in Fig. 3, provide insights into the surface functional groups of the materials. The spectrum of Raw-BC reveals an heterogeneous chemical structure with numerous functional groups and aromatic rings, resembling oxidized graphitized carbons [46] and pseudo-lignins [47]. This complex spectrum arises from the overlap of adsorption bands assigned to stretching and bending modes of various functional groups on carbon surfaces (C=O, C–O, C–O–C, C–C, C=C, C–H, etc.). These bands indicate the presence of oxygen double-

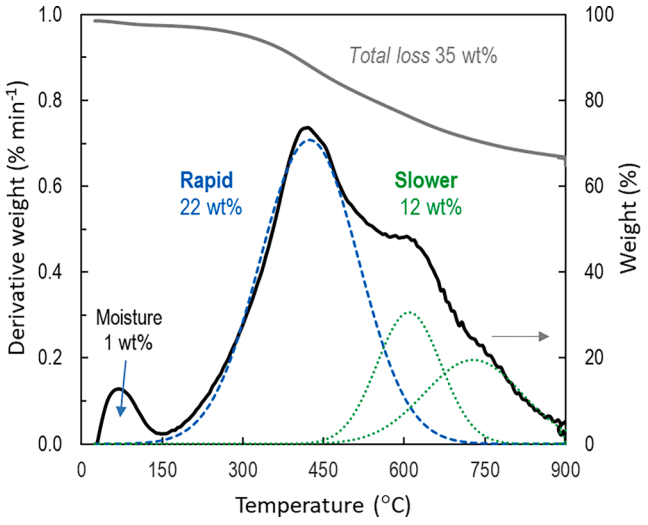

Fig. 2. Thermogravimetric profile of raw carbon material (Raw-BC) degradation under N_2 flow (50 mL min^{-1}) with a heating rate of 5 °C min^{-1}.

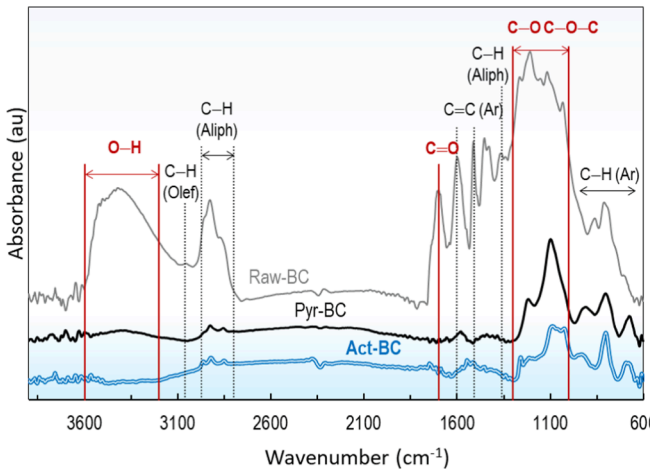

Fig. 3. FTIR spectra of raw bio-oil derived carbon material (Raw-BC), pyrolyzed carbon material (Pyr-BC) and activated carbon (Act-BC) in the 3800–600 cm^{-1} region.

bonded to carbon (C=O) in lactones, aldehydes or carboxylic moieties within conjugated systems (around 1700 cm^{-1}) [48], lignin-derived moieties (around 1445 cm^{-1}) [49], and syringyl and guaiacyl rings (1000–1300 cm^{-1}) [50]. Additionally, the strong and broad band observed at 3200–3600 cm^{-1} can be attributed to the stretching of hydroxyl (O–H) in alcohols, phenols and carboxylic acids [51]. The presence of aromatic structures in the carbon materials is confirmed by the band at ca. 1600 cm^{-1} (associated with C=C in highly condensed aromatics and dienes) [42], the bands ranging from 675 to 900 cm^{-1} (related to the out-of-plane bending of aromatic C–H bonds) [47], and the bands at 1490–1530 cm^{-1} (C=C in low condensed aromatics) [52].

The FTIR spectra of pyrolyzed carbon (Pyr-BC) and activated carbon (Act-BC) provide evidence of the chemical transformations occurring during pyrolysis and activation treatments, respectively. The absorbance intensity follows the order Raw-BC ≫ Pyr-BC > Act-BC, indicating changes in the carbon structure due to the removal of labile oxygen-containing functional groups. The band at 1700 cm^{-1}, representing the C=O stretch in ketones, aldehydes and carboxylic acid groups, decreased significantly. The broad hydroxyl band (3400 cm^{-1}) vanished completely, indicating the dehydration of hydroxyl groups, possibly due to a reduction in phenolic OH content, which is also supported by the decrease in the 1360 cm^{-1} band (associated with phenolic O–H and aliphatic C–H in CH_3). This could be attributed to repolymerization, considering the dissociation energy of phenolic OH from the benzene ring [53].

Additionally, the results reveal that a higher relative abundance of bands was associated with aromatic bonds. These findings imply that these carbon materials have a greater homogeneity of functional groups compared to Raw-BC, with oxygen likely present in C–O and C–O–C structures. In Fig. 4, the possible structure of these materials is presented based on the FTIR results.

3.2.2. Morphology and textural properties

The SEM images of Raw-BC, Pyr-BC, and Act-BC samples collected at increasing magnifications (500x, 3kx, and 10kx), are compared in Fig. 5. These images highlight significant differences in the surface morphology of these carbon materials. Raw-BC (Fig. 4a-c) exhibits a relatively uniform morphology with low porosity and irregular, rounded fractural edges. The development of porosity after the pyrolysis and activation treatment is clearly evidenced by the SEM images of Pyr-BC (Fig. 4d–f) and Act-BC (Fig. 4g–i). These samples exhibit a highly cracked surface at the micrometer scale.

The findings obtained from the SEM images align with the textural properties determined by gas physisorption. The adsorption–desorption isotherms and pore size distribution profiles of Pyr-BC and Act-BC are presented in Fig. 6. The textural properties, including specific surface area, micropore volume, and average pore width, are summarized in Table 2. No porosity was detected in Raw-BC material. The pyrolysis treatment generated a significant surface area of 595 $m^2\ g^{-1}$ in the carbon material, along with a micropore volume of 0.16 mL g^{-1}. Upon activation, both the surface area and the micropore volume in Act-BC substantially increased to 1070 $m^2\ g^{-1}$ and 0.41 mL g^{-1}, respectively. This carbon exhibits a type I adsorption isotherm, i.e., the characteristic of highly microporous materials. Furthermore, the results confirm that the pyrolysis treatment creates narrow micropores with an average pore size of 0.48 nm, while further activation leads to the formation of wider micropores with an average size of 0.81 nm.

The characterization results provide evidence that the activation process, involving pyrolysis-alkaline treatment-carbonization (as described in Section 2.2) induces significant changes in the composition and structure of the carbon material derived from bio-oil. The resulting material, Act-BC, exhibits a substantial specific surface area and significant micropore volume, with textural properties resembling those reported for activated carbons [54] and steam-activated bio-chars [55].

3.3. Adsorption of pollutants

3.3.1. Methylene blue

The adsorption effectiveness of Raw-BC, Pyr-BC, and Act-BC carbon materials for the removal of MB from wastewater was evaluated in terms of adsorption capacity (Q_e, mg g_{BC}^{-1}) and removal ratio (R, %), according to Eq. (1) and Eq. (2), respectively. The results, depicted in Fig. 7, represent the average values obtained from three experiments for each carbon sample.

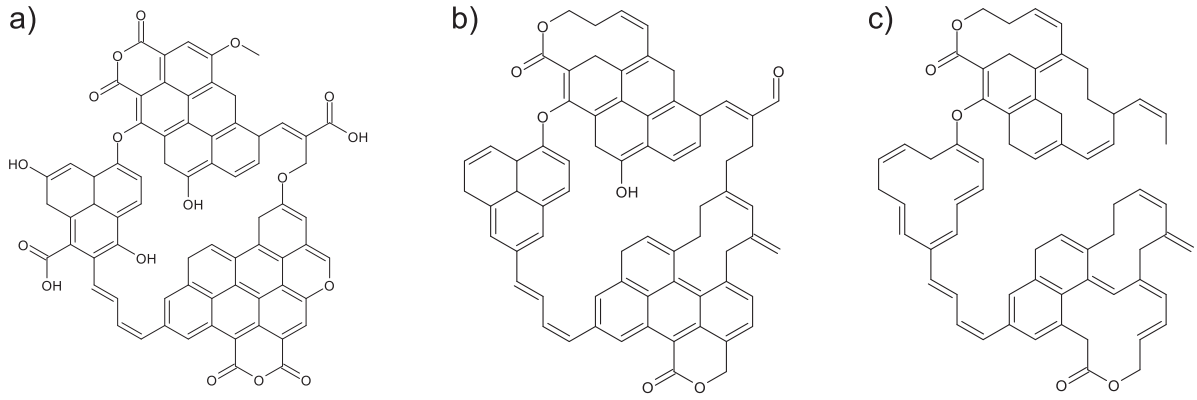

Fig. 4. Proposed chemical structure of a) raw bio-oil derived carbon material (Raw-BC), b) pyrolyzed carbon material (Pyr-BC), and c) activated carbon (Act-BC).

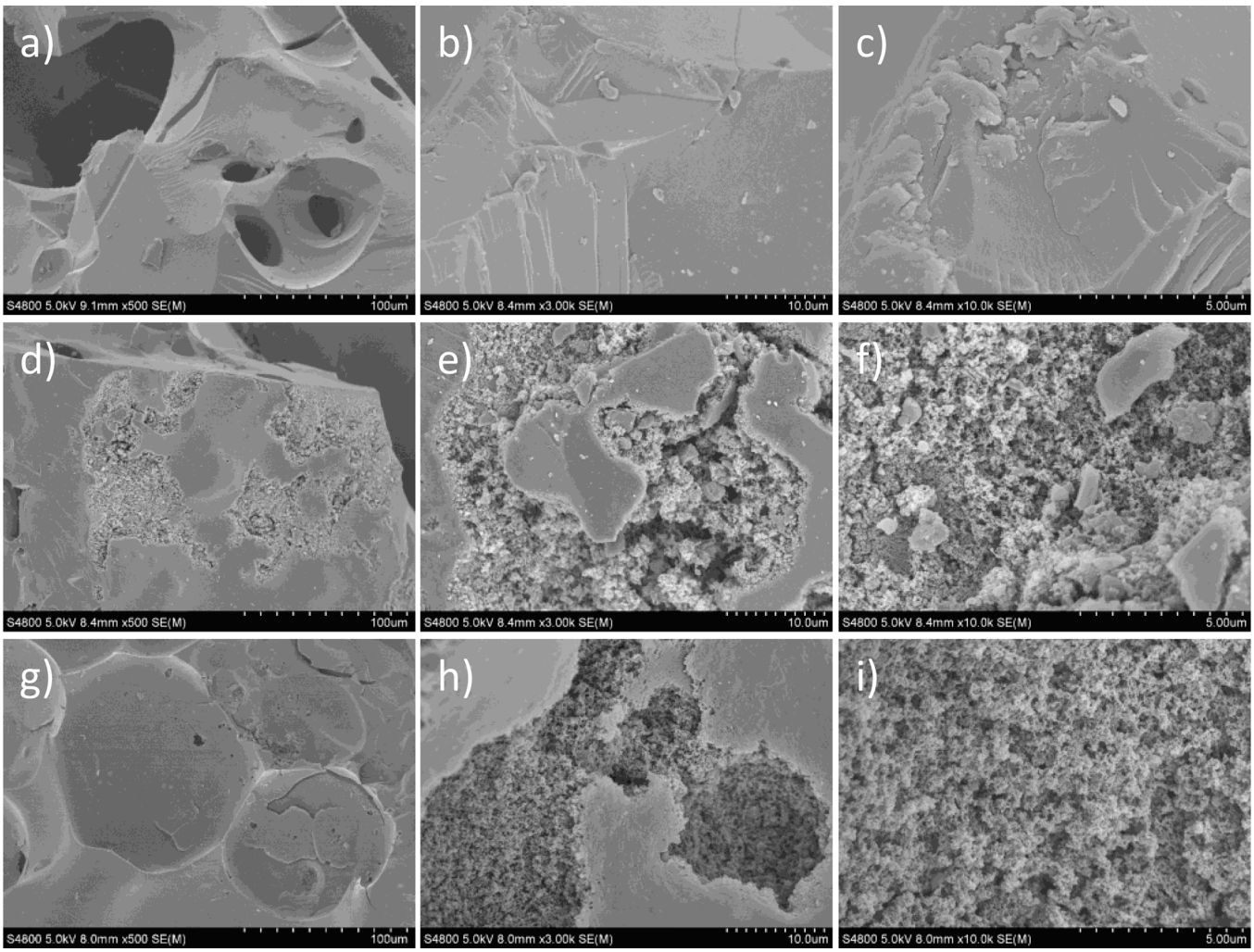

Fig. 5. Morphology and microstructure of Raw-BC (a – c), pyrolyzed material Pyr-BC (d – f) and activated carbon Act-BC (g – i).

The adsorption capacity of Raw-BC was initially evaluated and found to be ineffective for MB removal even after a 24-hour contact time. This result indicates that despite the presence of numerous oxygen-containing functional groups in Raw-BC, as revealed by FTIR results (Fig. 3), the negligible porosity of this material does not facilitate surface chemisorption reactions. The adsorption tests of Pyr-BC also indicate ineffective MB removal despite its higher surface area and micropore volume (Table 2). This suggests that the micropores developed in Pyr-BC are very narrow, with an average pore width of 0.48 nm, hindering the access and diffusion of MB molecules within the adsorbent internal structure. However, it should be noted that these properties might be advantageous in gas-phase applications, such as separation or gas cleaning [56].

The results with Act-BC confirm its effectiveness for MB adsorption (Fig. 7). Rapid adsorption occurs during the first 2 h of contact, attributing to the fast diffusion of MB molecules. A removal ratio of 50 % of the contaminant from the wastewater is achieved, with an adsorption capacity of 2.81 $mg_{MB}\ g^{-1}_{Act\text{-}BC}$. After 2 h, the adsorption efficiency decreases, leading to a MB removal ratio of approximately 80 % after 8 h of contact time. Afterwards, a nearly asymptotic trend is observed, reaching a final concentration of MB in wastewater of 0.7 $mg_{MB}\ L^{-1}$ after 24 h of contact. This corresponds to a 98 % removal ratio and an adsorption capacity of 5.7 $mg_{MB}\ g^{-1}_{Act\text{-}BC}$. Our results align with the values of removal ratio and adsorption capacity reported by Mussa et al. [30] in a comprehensive review focused on the design of biosorbents for the removal of MB.

These findings emphasize the crucial role that micropore size plays in the MB adsorption mechanism. Effective adsorption of this pollutant requires a carbon material with an appropriate pore width, allowing molecules to access the internal pore structure where they are captured. Thus, the activation procedure involving pyrolysis-alkaline treatment-carbonization, employed in this study, not only enhances the surface area of Raw-BC but also develops a porous structure with the suitable width range for effective MB adsorption.

3.3.2. *Hexavalent chromium*

The adsorption effectiveness of the three carbon materials for the removal of hexavalent chromium (Cr(VI)) from wastewater was initially evaluated for a contact time of 24 h. The corresponding values of adsorption capacity and removal ratio are presented in Table 3, along with the remaining concentration of Cr(VI) (note that the initial concentration of Cr(VI) solution was 100 mg L^{-1}).

The results align with those obtained for the MB dye, as both Raw-BC and Pyr-BC materials exhibit poor Cr(VI) adsorption capacity compared to Act-BC. This activated carbon demonstrates the ability to remove approximately 47 % of the pollutant from the wastewater solution, resulting in a final concentration below 54 $mg_{Cr(VI)}\ L^{-1}$. This corresponds to an adsorption capacity of 7.6 $mg_{Cr(VI)}\ g^{-1}$. It is noteworthy that despite the aforementioned limitations in porosity for Raw-BC and Pyr-BC, which render them ineffective for MB removal, these materials manage to remove over 6 % of Cr(VI) from the pollutant solution (Table 3). This result can be attributed to surface complexation

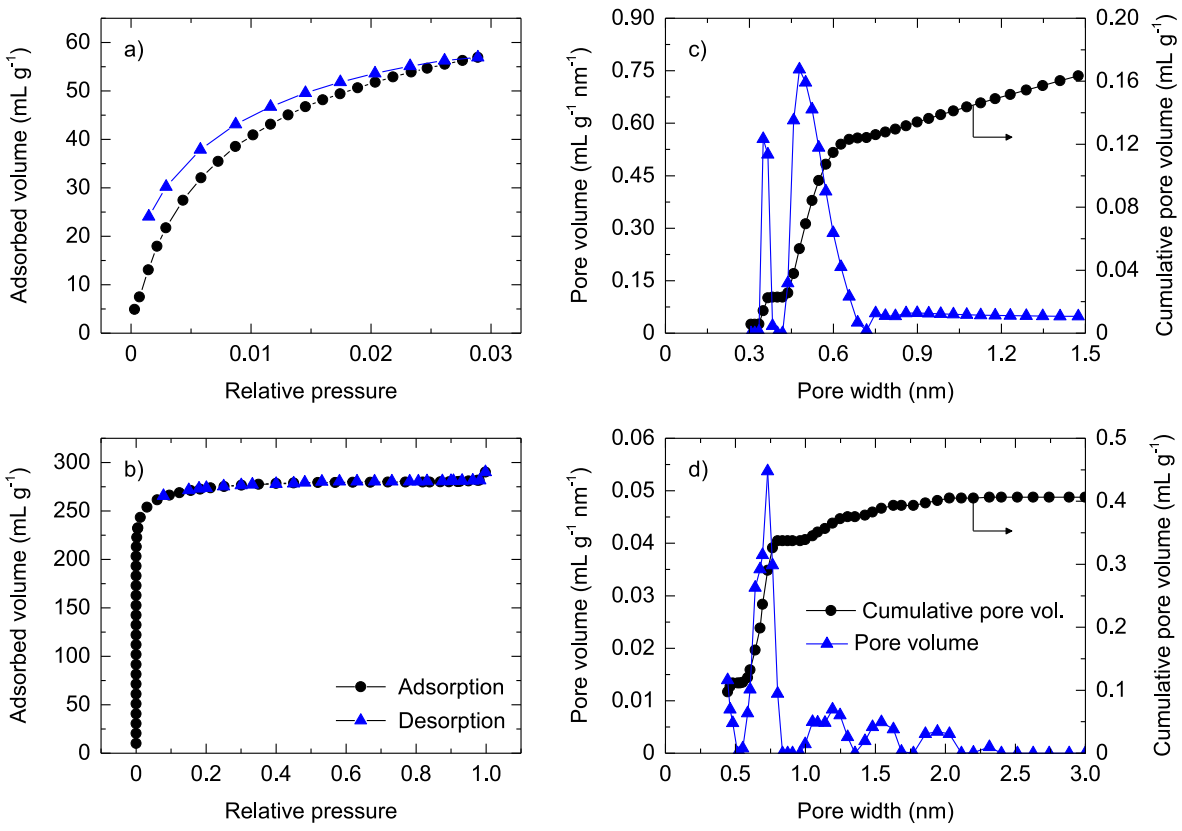

Fig. 6. Adsorption-desorption isotherms of (a) Pyr-BC (CO_2, 0 °C) and (b) Act − BC (N_2, −196 °C). NDFT pore width distribution of (c) Pyr-BC and (d) Act-BC.

Table 2
Textural properties of pyrolyzed Pyr-BC and activated carbon Act-BC.

Sample	Surface area ($m^2\ g^{-1}$)	Micropore volume ($mL\ g^{-1}$)	Average pore width (nm)
Pyr-BC[(a)]	595	0.16	0.48
Act-BC[(b)]	1070	0.41	0.81

[(a)] CO_2 physisorption at 0 °C; [(b)] N_2 physisorption at −196 °C

phenomena occurring during the adsorption of heavy metals [57]. The –COC and –C=O functional groups (Fig. 3) can interact with chromium ions, forming multi-atom structures [58], thereby enhancing the adsorption process.

The results of Cr(VI) adsorption with Act-BC may appear low compared to values reported by other authors using biomass-derived adsorbents [59,60]. However, it is important to note that those studies were mostly conducted under strongly acidic conditions (pH around 2.0) to enhance the adsorption of this heavy metal [61]. In this work, adsorption tests were carried out neither using chemical reagents to modify the pH nor continuous stirring. Consistent with our findings, Valentin-Reyes et al. [34] emphasized the importance of pH in the removal of hexavalent chromium from aqueous solutions and reported adsorption capacity values in the 6.5–7 mg/g range for commercial activated carbon modified by thermal treatment at 800–900 °C.

It should be highlighted that, despite most studies on Cr(VI) removal being conducted at the laboratory scale, the procedure employed in this study is more applicable to the decontamination of real industrial wastewater than methods that require acidification. The need to use chemicals and more labor-intensive methods for the required acidification (and subsequent basification to neutral pH) would render the process economically and environmentally unfeasible.

The impact of contact time on the effectiveness of Act-BC in removing Cr(VI) from wastewater is depicted in Fig. 8 (each data point represents the average of three experiments). The results reveal that the highest Cr(VI) removal rate occurs within the first hour, indicating rapid diffusion of chromium ions through the porous structure of Act-BC, resulting in an approximately 15 % removal. Subsequently, the adsorption rate gradually decreases, showing three distinct intervals (0–1 h, 1–4 h, and 4–24 h). Consequently, a 25.6 % removal of Cr(VI) is achieved after 4 h of contact, increasing up to 46.5 % at 24 h.

It is important to note that both the trends of Cr(VI) removal ratio (R) and adsorption capacity (Q_e) indicate that longer contact times are necessary to achieve the maximum values of pollutant removal. This can be attributed to the considerably higher initial concentration of Cr(VI) solution (100 mg L^{-1}) compared to that used for MB (35 mg L^{-1}), for which the maximum values were attained (as shown in Fig. 7).

3.4. Recyclability of bio-oil derived activated carbon

The recyclability of an activated carbon, especially its capability to undergo multiple adsorption–desorption cycles, is a crucial aspect that can enhance the attractiveness of bio-based adsorbents. In this section, the results obtained from evaluating the regeneration capacity of Act-BC for the adsorption of MB in four consecutive adsorption–desorption cycles are presented (Fig. 9). MB was selected as the pollutant for this study since desorption of Cr(VI) would involve surface complexation phenomena.

The results show a decrease in adsorption capacity after the intermediate desorption (regeneration) process. This effect is more noticeable in the initial cycles but becomes less evident after the third cycle. It suggests that, although there is an irreversible loss of activity, the regenerated adsorbent could potentially reach a stable state (equilibrium), enabling reproducible results in subsequent adsorption-regeneration cycles.

Furthermore, the regeneration procedure significantly impacts the adsorption dynamics of MB, particularly affecting the initial adsorption

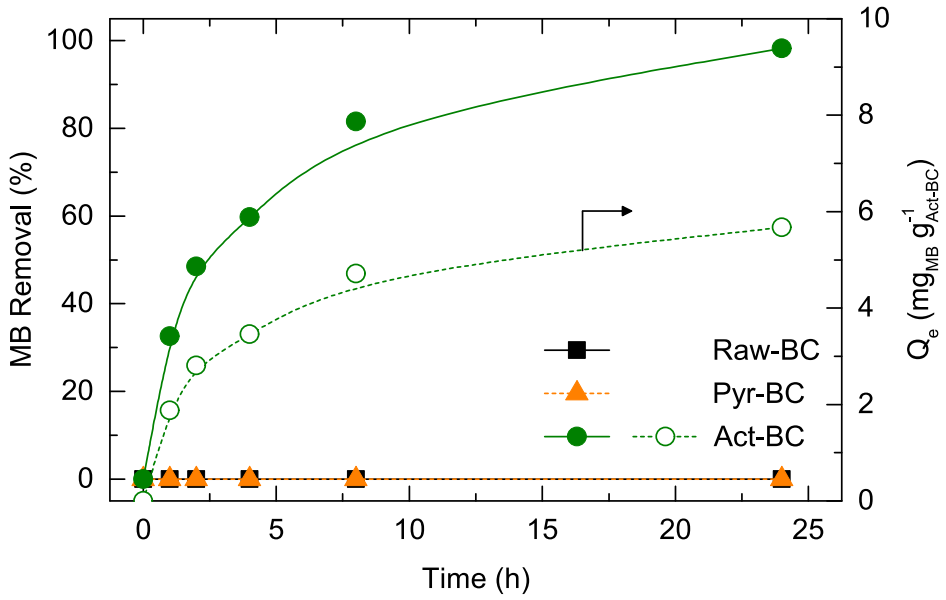

Fig. 7. Evolution over time of MB removal ratio achieved with Raw-BC, Pyr-BC and Act-BC (%, left axis). Evolution over time of Act-BC adsorption capacity (Q_e, right axis).

Table 3
Removal ratio (R), remaining concentration (Ce), and adsorption capacity (Qe) of Cr(VI) achieved with each carbon material after 24 h of contact time.

Sample	R (%)	C_e ($mg_{Cr(VI)}$ L^{-1})	Q_e ($mg_{Cr(VI)}$ g_{BC}^{-1})
Raw-BC	6.4	93.6	1.1
Pyr-BC	6.6	93.4	1.1
Act-BC	46.5	53.5	7.6

rate. The rate observed during short contact times (below 2 h) decreases after each cycle, while the rate appears to be consistent above 2 h, regardless of the cycle (Fig. 9). Consequently, the amount of MB removed in the fourth cycle (approximately 90 %) is slightly lower than in the first cycle (approximately 98 %) for contact times of 24 h. This behavior can be attributed to pore blockage resulting from incomplete desorption of MB molecules, which remain adsorbed in the microporous structure of Act-BC (irreversible saturation).

The Act-BC shows a promising recyclability under the conditions studied, demonstrating a slight loss of adsorption capacity in four testing cycles. It shows higher recovery than other carbon-based adsorbents after desorption using water (30 % in three cycles [62]), methanol (75 % in six cycles [63]) and acids (75–80 % in 2–5 cycles [64,65]). Our results align with those reported employing desorption as regeneration technique using different alcohol/acid mixture solutions (60–91 % in 3–6 cycles [66–68]).

The studies on the reusability of carbon-based adsorbents evidence that the efficiency of the regeneration process through desorption strongly depends on the liquid medium, indicating the potential to optimize the regeneration of Act-BC and to minimize irreversible loss of activity. Methanol, ethanol, acetic acid, and NaOH are among the most investigated media used to facilitate desorption of MB.

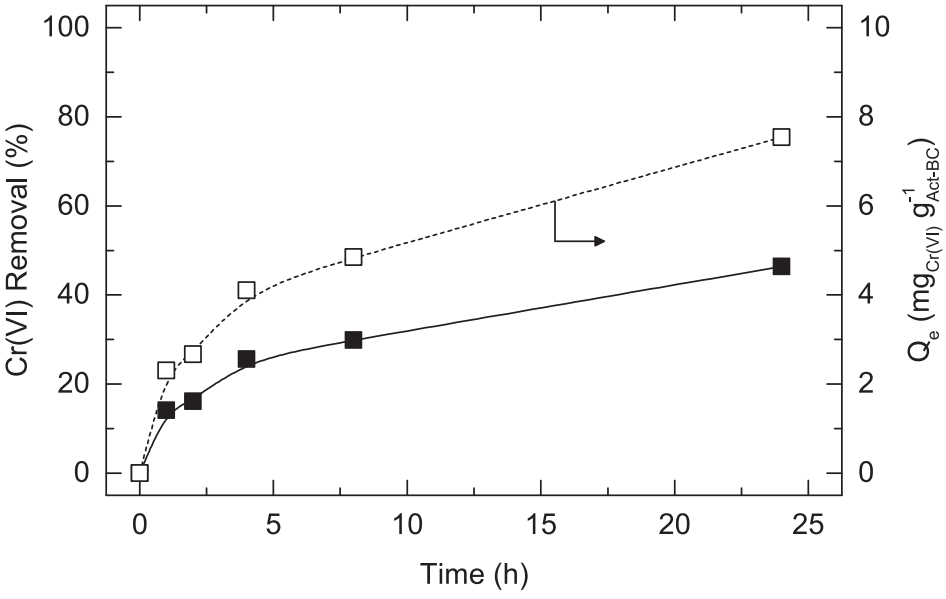

Fig. 8. Evolution over time of Cr(VI) removal ratio and adsorption capacity (Q_e) achieved with Act-BC.

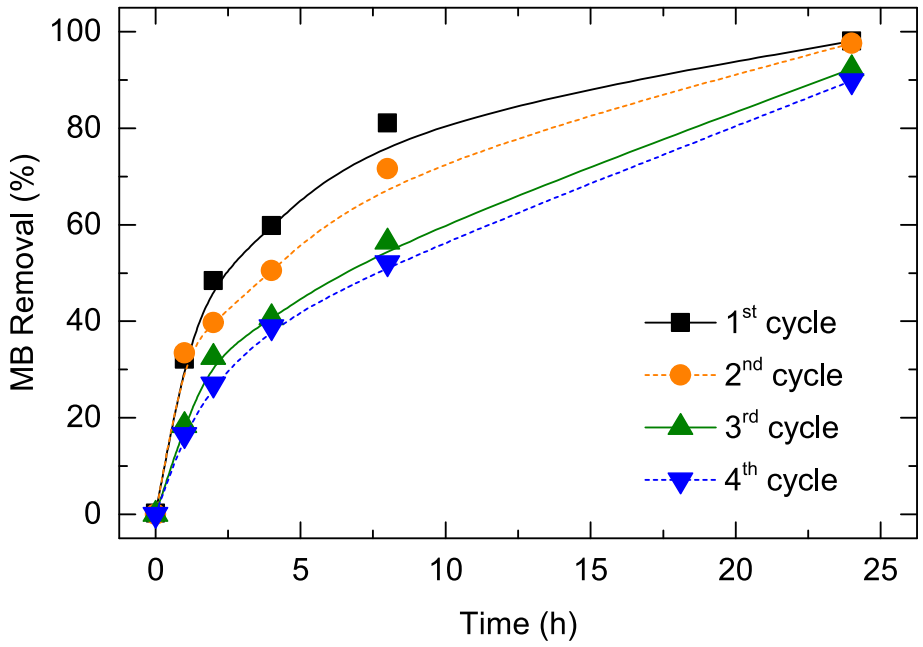

Fig. 9. Recyclability of Act-BC for methylene blue (MB) removal in four adsorption–desorption cycles. (For interpretation of the references to colour in this figure legend, the reader is referred to the web version of this article.)

3.5. Adsorption kinetics

The adsorption of pollutant species in wastewater generally follows a four-step pathway: "transfer to adsorbent surface−diffusion through liquid film−intraparticle diffusion−intrinsic adsorption". To gain knowledge on the adsorption of MB by the synthesized Act-BC material, we initially assessed the effectiveness of surface reaction models (SRM) in fitting the adsorption data. These widely used models assume that the physical/chemical interaction between pollutant molecules and carbon binding sites (intrinsic adsorption) is the rate-controlling step in the adsorption process. The linearized equations of the pseudo-first order (PFO) model and pseudo-second order (PSO) model are the most commonly applied.

$$PFO\Rightarrow \quad \log(Q_e - Q_t) = \log Q_e - \left(\frac{K_1}{2.303}\right)\cdot t \tag{3}$$

$$PSO\Rightarrow \quad \frac{t}{Q_t} = \frac{1}{K_2 Q_e^2} + \frac{t}{Q_e} \tag{4}$$

where Q_e refers to the adsorption capacity at equilibrium (mg g^{-1}), Q_t is the amount of pollutant adsorbed (mg g^{-1}) at any time t (min), K_1 is the pseudo-first-order rate constant (min^{-1}) and K_2 is the pseudo-second-order rate constant (g mg^{-1} min^{-1}).

The degree of agreement between the experimental data and the model-predicted values was quantified using correlation coefficients (R^2), where values approaching 1 indicate a strong conformity. The experimental adsorption curves and fitting parameters are presented in Fig. 10 and Table 4, respectively. The results indicate that the adsorption of MB by Act-BC can be explained by the pseudo-first-order (PFO) kinetic model, except for the last 3 h. During this period, the more accessible pores of the carbon material become saturated with MB

Table 4
Parameters of the pseudo-first order (PFO) and pseudo-second order (PSO) models for MB adsorption by Act-BC.

Model	$Q_{e,\ exp}$	$Q_{e,\ calc}$	Rate Constant		R^2	$1-R^2$
			K_1	K_2		
PFO	5.78	5.39	0.00201		0.971	0.029
PSO	5.78	6.31		1.02193	0.998	0.002

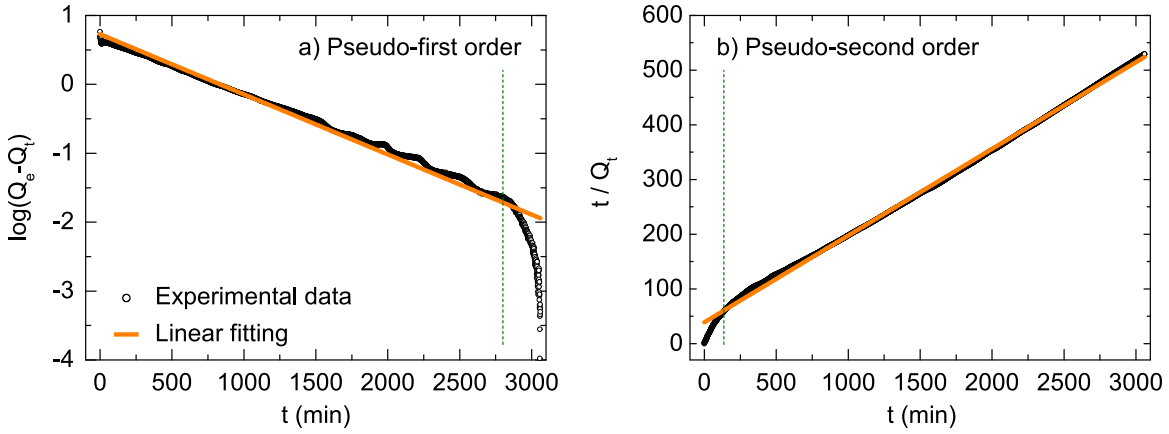

Fig. 10. Fitting results of (a) pseudo-first order kinetic model and (b) pseudo-second order kinetic model for adsorption of MB by Act-BC.

molecules, making pore diffusion the rate-controlling step. This effect can be attributed to the highly microporous nature of this material (Table 2).

Fig. 10b demonstrates that, except for the first 2 h, the adsorption of MB is well described by the pseudo-second-order (PSO) kinetic model, reaching an overall fitting correlation coefficient of 0.998, which is higher than that of the pseudo-first-order (PFO) model ($R^2 = 0.971$). This evidences the influence of chemisorption phenomena in the adsorption process, such as complexation and coordination [69]. In terms of adsorption capacity, the values predicted by both models are close to the experimental value (Table 4), although in the case of PFO, the difference is smaller.

These results evidence that the linearized versions of surface reaction models (SRM), which focus on intrinsic adsorption (i.e., the physico-chemical interaction between the adsorbent binding site and pollutant), might not accurately predict pollutant removal throughout the adsorption process. A marginal difference in R^2 does not always justify a better fit to the experimental data [35]. To overcome these limitations, Mas Transfer Modelling (MTM) was applied to study the adsorption kinetics. These models assume that the intrinsic adsorption reaction is fast enough so that the rate-determining steps can be the diffusion of pollutant species from the bulk to the external surface of the adsorbent (film diffusion) and/or the diffusion of pollutants within the micropores to the adsorbent binding sites (intraparticle diffusion). In order to elucidate the influence of these phenomena on the adsorption process, the adequacy of liquid film diffusion model (LFD) and Bangham's pore diffusion model (BPD) was assessed. The linear forms of these models are represented by Eq. (5) and Eq. (6), respectively. The fitting parameters of these models provide insights into the involvement of liquid film diffusion and intraparticle diffusion mechanisms in the adsorption process [70,71].

$$LFD \Rightarrow \ln\left(1 - \frac{Q_t}{Q_e}\right) = -K_{LF}t \tag{5}$$

being Q_e the adsorption capacity at equilibrium (mg g^{-1}), Q_t the adsorption capacity (mg g^{-1}) at time t (min) and K_{LF} the liquid diffusion constant (min^{-1}).

$$BPD \Rightarrow \log\left(\frac{C_0}{C_0 - mQ_t}\right) = \log\left(\frac{mK_\beta}{2.303V}\right) + \Delta\beta \log t \tag{6}$$

where C_0 is the initial MB concentration (mg L^{-1}), V is the volume of solution (mL), m the weight of Act-BC adsorbent (g L^{-1}), $\Delta\beta$ and K_β are the Bangham's constants (obtained as slope and y-intercept).

The curves representing the experimental adsorption data and the fitting parameters of the Mass Transfer Models (MTM) are presented in Fig. 11, and the corresponding results are summarized in Table 5. Except for the last 3 h (Fig. 11a), the Liquid Film Diffusion (LFD) model demonstrates a good fit to the adsorption data, with a y-intercept value close to zero [72]. These findings suggest that liquid film diffusion plays a role in the adsorption process of MB by Act-BC, although it cannot be considered the rate-determining step, given the significant difference between the experimental and calculated values of adsorption capacity Q_e (Table 5). Furthermore, the results from applying the Bangham's Pore Diffusion (BPD) model (Fig. 11b) exhibit a relatively high overall correlation coefficient ($R^2 > 0.9$, Table 5), particularly in the last 3 h (up to $R^2 = 0.989$) where the pseudo-first order model fails (Fig. 10a). This confirms the involvement of liquid pore diffusion limitation in the adsorption of the MB pollutant.

Based on these results, it can be affirmed that chemisorption is the most limiting stage in the adsorption rate of MB by Act-BC, as indicated by the good fit to a pseudo-second order equation. However, physisorption and liquid film diffusion also play a role. These stages notably influence the adsorption rate during the first 2 h, as evidenced by the best fit of the Pseudo-First Order (PFO) and Liquid Film Diffusion (LFD) models. After 48 h, intraparticle pore diffusion becomes the rate-controlling step, as supported by the suitability of the Bangham's Pore Diffusion (BPD) model. This shift can be attributed to the highly microporous nature of the material and the reduction in available active sites for adsorption due to Act-BC saturation.

3.6. Overcoming challenges in commercial application

The successful translation of research findings into practical applications is a critical step in the development of bio-based activated carbons for pollutant removal. While our study has demonstrated a remarkable efficiency of the synthesized activated carbon in adsorbing methylene blue and hexavalent chromium, the real-world implementation demands careful consideration of the challenges that may be encountered.

A noteworthy concern is the time required to reach equilibrium, a factor with implications for the operational efficiency of the adsorption process. In real-world applications, the extended duration may hinder the material's applicability for industries requiring rapid wastewater

Table 5
Parameters of the Liquid Film Diffusion (LFD) and Bangham's Pore Diffusion (BPD) for MB adsorption by Act-BC.

Model	$Q_{e,\,exp}$	$Q_{e,\,calc}$	$\Delta\beta$	Rate Constant		R^2	$1-R^2$
				K_{LF}	K_β		
LFD	5.78	2.66		0.002		0.971	0.029
BPD	5.78		0.66072		0.01108	0.953	0.047

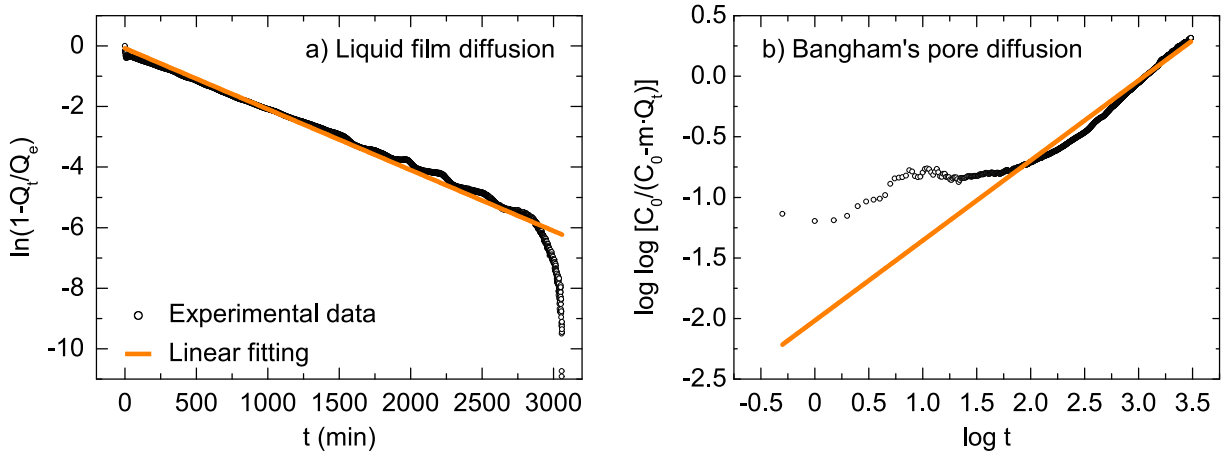

Fig. 11. Fitting results of (a) Liquid Film Diffusion model and (b) Bangham's Pore Diffusion model for adsorption of MB by Act-BC.

treatment to meet regulatory standards. To address this, one potential strategy involves the incorporation of catalysts during the activated carbon synthesis, which could enhance the adsorption kinetics and mitigate the impact of extended equilibrium times. However, a delicate balance between kinetics and adsorption efficiency must be struck. Rapid adsorption kinetics should not compromise the material's overall pollutant removal capacity. Achieving this balance is essential to ensure that the material remains competitive and viable for a wide range of pollutant concentrations and applications. Future research efforts should be directed towards optimizing the bio-based carbon performance by exploring potential synergies between rapid kinetics and high adsorption efficiency.

The recyclability of the synthesized activated carbon is also a key factor for its practical viability. Although our study demonstrated stable behavior in four adsorption-regeneration cycles, further research could be conducted to refine regeneration processes, ensuring that the material keeps high efficiency over multiple cycles. Developing efficient and cost-effective recovery processes will enhance the reusability, reducing the demand for fresh adsorbents and contributing to economic feasibility.

Different industries and pollutant scenarios may present unique challenges. Understanding and addressing these application-specific challenges are crucial for the successful commercialization of the proposed material. Further exploration of its effectiveness in diverse industrial scenarios and with a broader range of pollutants will provide valuable insights and enhance its applicability.

In conclusion, while our research presents promising results for the development of a sustainable material for wastewater treatment, its commercial application requires strategic considerations and targeted research efforts. Addressing the challenges outlined above and exploring potential solutions will be essential for broadening the applicability of the synthesized activated carbon in real-world industrial settings.

4. Conclusions

This study effectively addresses the challenge of carbon deposition during bio-oil processing. Our methodology enables the valorization of carbon residue into porous material with a specific surface area of 1070 $m^2\ g^{-1}$ and a micropore volume of 0.41 mL g^{-1}. The efficient valorization process contributes to the enhanced carbon efficiency of bio-oil transformation, reducing waste and improving process sustainability and economic viability.

The synthesized activated carbon demonstrates remarkable efficiency in adsorbing pollutants, achieving a removal ratio of 98 % for methylene blue and 47 % for hexavalent chromium. For methylene blue, the adsorption capacity reaches 5.7 mg g^{-1}, emphasizing the potential of the material in wastewater treatment applications.

We evaluated the recyclability of the activated carbon, showing its potential for regeneration and reuse in multiple adsorption–desorption cycles. Despite a decrease in adsorption capacity after regeneration, the material exhibits stable behavior after the third cycle, with a removal ratio of approximately 90 %. This feature minimizes the demand for fresh adsorbents, enhancing economic feasibility and overall sustainability.

Through extensive studies on adsorption kinetics, we gained valuable insights into the fundamental phenomena involved in the adsorption process. Chemisorption is identified as the most limiting stage in the adsorption rate, although physisorption and liquid film diffusion also play a role, especially at short solid–liquid contact times (up to 2 h). For longer contact times (above 48 h), intraparticle pore diffusion becomes the rate-controlling step due to the highly microporous nature of the activated carbon and the reduction in available active sites.

The outcomes of this study provide crucial information for the development of sustainable materials for wastewater treatment. Exploring similar valorization methods for other biomass-derived residues and broadening the range of pollutants will further contribute to reduce environmental impact and promoting green technologies across various industrial sectors. The integration of these quantitative findings into future studies will pave the way for advancements in the field of sustainable materials and wastewater treatment.

CRediT authorship contribution statement

Beatriz Valle: Writing – review & editing, Writing – original draft, Funding acquisition, Conceptualization. **Eriz Corro:** Visualization, Investigation, Formal analysis. **Roberto Palos:** Writing – review & editing, Writing – original draft, Visualization. **Iratxe Crespo:** Investigation, Formal analysis. **M. Mirari Antxustegi:** Investigation, Formal analysis, Supervision. **Pedram Fatehi:** Writing – review & editing. **María González-Alriols:** Supervision, Funding acquisition.

Declaration of competing interest

The authors declare that they have no known competing financial interests or personal relationships that could have appeared to influence the work reported in this paper.

Data availability

Data will be made available on request.

Acknowledgements

This work was supported by the Ministry of Science and Innovation of the Spanish Government [grant RTI2018-095990-J-I00 funded by MCIN/AEI/10.13039/501100011033 "ERDF A way of making Europe"], the European Commission [H2020-MSCA RISE 2018 contract No. 823745], the Basque Government [grant IT1645-22], the University of the Basque Country UPV/EHU [grant UPV/EHU PIF 2021 of Iratxe Crespo] and Gipuzkoa's Provincial Government [grant "Etorkizuna Eraikiz" 2022/2023].

Appendix A. Supplementary data

Supplementary data to this article can be found online at https://doi.org/10.1016/j.fuel.2024.130994.

References

[1] Dragone G, Kerssemakers AAJ, Driessen JLSP, Yamakawa CK, Brumano LP, Mussatto SI. Innovation and strategic orientations for the development of advanced biorefineries. Bioresour Technol 2020;302:122847. https://doi.org/10.1016/j.biortech.2020.122847.

[2] Hu X, Gholizadeh M. Progress of the applications of bio-oil. Renewable Sustainable Energy Rev 2020;134:110124. https://doi.org/10.1016/j.rser.2020.110124.

[3] Shan Ahamed T, Anto S, Mathimani T, Brindhadevi K, Pugazhendhi A. Upgrading of bio-oil from thermochemical conversion of various biomass – Mechanism, challenges and opportunities. Fuel 2021;287:119329. https://doi.org/10.1016/j.fuel.2020.119329.

[4] Carpenter D, Westover TL, Czernik S, Jablonski W. Biomass feedstocks for renewable fuel production: a review of the impacts of feedstock and pretreatment on the yield and product distribution of fast pyrolysis bio-oils and vapors. Green Chem 2014;16:384–406. https://doi.org/10.1039/C3GC41631C.

[5] Michailof CM, Kalogiannis KG, Sfetsas T, Patiaka DT, Lappas AA. Advanced analytical techniques for bio-oil characterization, Wiley Interdiscip Rev. Energy Environ 2016;5:614–39. https://doi.org/10.1002/wene.208.

[6] A. Kumar, J.P. Chakraborty, R. Singh, Bio-oil: the future of hydrogen generation, in: Biofuels, Taylor and Francis Ltd., 2017: pp. 663–674. https://doi.org/10.1080/17597269.2016.1141276.

[7] Valle B, Remiro A, García-Gómez N, Gayubo AG, Bilbao J. Recent research progress on bio-oil conversion into bio-fuels and raw chemicals: a review. J Chem Technol Biotechnol 2019;94:670–89. https://doi.org/10.1002/jctb.5758.

[8] Hu X, Zhang Z, Gholizadeh M, Zhang S, Ho Lam C, Xiong Z, et al. Coke formation during thermal treatment of bio-oil. Energy Fuels 2020;34:7863–914. https://doi.org/10.1021/acs.energyfuels.0c01323.

[9] Valle B, Castaño P, Olazar M, Bilbao J, Gayubo AG. Deactivating species in the transformation of crude bio-oil with methanol into hydrocarbons on a HZSM-5 catalyst. J Catal 2012;285:304–14. https://doi.org/10.1016/j.jcat.2011.10.004.

[10] Ibáñez M, Valle B, Bilbao J, Gayubo AG, Castaño P. Effect of operating conditions on the coke nature and HZSM-5 catalysts deactivation in the transformation of crude bio-oil into hydrocarbons. Catal Today 2012;195:106–13. https://doi.org/10.1016/j.cattod.2012.04.030.

[11] Cordero-Lanzac T, Palos R, Hita I, Arandes JM, Rodríguez-Mirasol J, Cordero T, et al. Revealing the pathways of catalyst deactivation by coke during the hydrodeoxygenation of raw bio-oil. Appl Catal B 2018;239:513–24. https://doi.org/10.1016/j.apcatb.2018.07.073.

[12] Hu X, Zhang Z, Gholizadeh M, Zhang S, Lam CH, Xiong Z, et al. Coke formation during thermal treatment of bio-oil. Energy Fuels 2020;34:7863–914. https://doi.org/10.1021/acs.energyfuels.0c01323.

[13] Gayubo A, Valle B, Aguayo A, Olazar M, Bilbao J. Pyrolytic lignin removal for the valorization of biomass pyrolysis crude bio-oil by catalytic transformation. J Chem Technol Biotechnol 2010;85:132–44. https://doi.org/10.1002/jctb.2289.

[14] Remiro A, Valle B, Aguayo AT, Bilbao J, Gayubo AG. Steam reforming of raw bio-oil in a fluidized bed reactor with prior separation of pyrolytic lignin. Energy Fuels 2013;27:7549–59. https://doi.org/10.1021/ef401835s.

[15] Valle B, Remiro A, Aramburu B, Bilbao J, Gayubo AG. Strategies for maximizing the bio-oil valorization by catalytic transformation. J Clean Prod 2015;88:345–8. https://doi.org/10.1016/j.jclepro.2014.06.017.

[16] Valle B, Aramburu B, Remiro A, Arandia A, Bilbao J, Gayubo AG. Optimal conditions of thermal treatment unit for the steam reforming of raw bio-oil in a continuous two-step reaction system. Chem Eng Trans 2017;57:205–10. https://doi.org/10.3303/cet1757035.

[17] Gayubo AG, Valle B, Aguayo AT, Olazar M, Bilbao J. Olefin production by catalytic transformation of crude bio-oil in a two-step process. Ind Eng Chem Res 2010;49:123–31. https://doi.org/10.1021/ie901204n.

[18] Katakojwala R, Venkata Mohan S. Multi-product biorefinery with sugarcane bagasse: process development for nanocellulose, lignin and biohydrogen production and lifecycle analysis, Chem. Eng J 2022;446:137233. https://doi.org/10.1016/j.cej.2022.137233.

[19] Dias M, Pinto J, Henriques B, Figueira P, Fabre E, Tavares D, et al. Nutshells as efficient biosorbents to remove cadmium, lead, and mercury from contaminated solutions. Int J Environ Res Public Health 2021;18:1–17. https://doi.org/10.3390/ijerph18041580.

[20] Rawat A, Srivastava A, Bhatnagar A, Gupta AK. Technological advancements for the treatment of steel industry wastewater: effluent management and sustainable treatment strategies. J Clean Prod 2023;383:135382. https://doi.org/10.1016/j.jclepro.2022.135382.

[21] Tang J, Liu Z, Liu W, Finfrock YZ, Ye Z, Liu X, et al. Application of Fe-doped biochar in Cr(VI) removal from washing wastewater and residual Cr(VI) immobilization in contaminated soil. J Clean Prod 2022;380:134973. https://doi.org/10.1016/j.jclepro.2022.134973.

[22] Seow YX, Tan YH, Mubarak NM, Kansedo J, Khalid M, Ibrahim ML, et al. A review on biochar production from different biomass wastes by recent carbonization technologies and its sustainable applications. J Environ Chem Eng 2022;10:107017. https://doi.org/10.1016/j.jece.2021.107017.

[23] Yang C, Wu H, Cai M, Li Y, Guo C, Han Y, et al. Valorization of food waste digestate to ash and biochar composites for high performance adsorption of methylene blue. J Clean Prod 2023;397:136612. https://doi.org/10.1016/j.jclepro.2023.136612.

[24] Ahmed MJ, Okoye PU, Hummadi EH, Hameed BH. High-performance porous biochar from the pyrolysis of natural and renewable seaweed (*Gelidiella acerosa*) and its application for the adsorption of methylene blue. Bioresour Technol 2019;278:159–64. https://doi.org/10.1016/j.biortech.2019.01.054.

[25] Zhou Y, Lu J, Zhou Y, Liu Y. Recent advances for dyes removal using novel adsorbents: a review. Environ Pollut 2019;252:352–65. https://doi.org/10.1016/j.envpol.2019.05.072.

[26] Thue PS, Lima DR, Lima EC, Teixeira RA, dos Reis GS, Dias SLP, et al. Comparative studies of physicochemical and adsorptive properties of biochar materials from biomass using different zinc salts as activating agents. J Environ Chem Eng 2022;10:107632. https://doi.org/10.1016/j.jece.2022.107632.

[27] Maheshwari K, Agrawal M, Gupta AB. Dye pollution in water and wastewater. In: Muthu SS, Khadir A, editors. Novel materials for dye-containing wastewater treatment. Sustainable textiles: production, processing, manufacturing & chemistry. Singapore: Springer; 2021. p. 1–25. https://doi.org/10.1007/978-981-16-2892-4_1.

[28] Yeamin MB, Islam MM, Chowdhury A-N, Awual MR. Efficient encapsulation of toxic dyes from wastewater using several biodegradable natural polymers and their composites. J Clean Prod 2021;291:125920. https://doi.org/10.1016/j.jclepro.2021.125920.

[29] Santoso E, Ediati R, Kusumawati Y, Bahruji H, Sulistiono DO, Prasetyoko D. Review on recent advances of carbon based adsorbent for methylene blue removal from waste water. Mater Today Chem 2020;16:100233. https://doi.org/10.1016/j.mtchem.2019.100233.

[30] Mussa ZH, Al-Ameer LR, Al-Qaim FF, Deyab IF, Kamyab H, Chelliapan S. A comprehensive review on adsorption of methylene blue dye using leaf waste as a bio-sorbent: isotherm adsorption, kinetics, and thermodynamics studies. Environ Monit Assess 2023;195:1–36. https://doi.org/10.1007/S10661-023-11432-1.

[31] Guleria A, Kumari G, Lima EC, Ashish DK, Thakur V, Singh K. Removal of inorganic toxic contaminants from wastewater using sustainable biomass: A review. Sci Total Environ 2022;823:153689. https://doi.org/10.1016/j.scitotenv.2022.153689.

[32] GracePavithra K, Jaikumar V, Kumar PS, SundarRajan P. A review on cleaner strategies for chromium industrial wastewater: Present research and future perspective. J Clean Prod 2019;228:580–93. https://doi.org/10.1016/j.jclepro.2019.04.117.

[33] Mohd. Rafatullah, Sulaiman O, Hashim R, Ahmad A. Adsorption of methylene blue on low-cost adsorbents: A review. J Hazard Mater 2010;177:70–80. https://doi.org/10.1016/j.jhazmat.2009.12.047.

[34] Valentín-Reyes J, García-Reyes RB, García-González A, Soto-Regalado E, Cerino-Córdova F. Adsorption mechanisms of hexavalent chromium from aqueous solutions on modified activated carbons. J Environ Manage 2019;236:815–22. https://doi.org/10.1016/j.jenvman.2019.02.014.

[35] Mahapatra U, Manna AK, Chatterjee A. A critical evaluation of conventional kinetic and isotherm modeling for adsorptive removal of hexavalent chromium and methylene blue by natural rubber sludge-derived activated carbon and commercial activated carbon. Bioresour Technol 2022;343:126135. https://doi.org/10.1016/j.biortech.2021.126135.

[36] Shi Y, Chang Q, Zhang T, Song G, Sun Y, Ding G. A review on selective dye adsorption by different mechanisms. J Environ Chem Eng 2022;10:108639. https://doi.org/10.1016/j.jece.2022.108639.

[37] Martelo N, Antxustegi M, Corro E, Baloch M, Volpe R, Gagliano A, et al. Use of residual lignocellulosic biomass for energetic uses and environmental remediation through pyrolysis. Energy Storage Saving 2022;1:129–35. https://doi.org/10.1016/j.enss.2022.04.004.

[38] Sanchez-Hachair A, Hofmann A. Hexavalent chromium quantification in solution: Comparing direct UV–visible spectrometry with 1,5-diphenylcarbazide colorimetry. C R Chim 2018;21:890–6. https://doi.org/10.1016/j.crci.2018.05.002.

[39] Rahim HU, Qaswar M, Wang M, Jing X, Cai X. Environmental applications of reduced sulfur species and composites in transformation and detoxification of contaminants. J Environ Chem Eng 2021;9:106696. https://doi.org/10.1016/j.jece.2021.106696.

[40] Antxustegi M, Corro E, Baloch M, Volpe R, Alriols MG. Production of activated biochars for wastewater treatment: characterization, activation and evaluation of the adsorption capacity. Chem Eng Trans 2022;92:547–52. https://doi.org/10.3303/cet2292092.

[41] Palos R, Gutiérrez A, Vela FJ, Maña JA, Hita I, Asueta A, et al. Assessing the potential of the recycled plastic slow pyrolysis for the production of streams attractive for refineries. J Anal Appl Pyrolysis 2019;142:104668. https://doi.org/10.1016/j.jaap.2019.104668.

[42] Ochoa A, Aramburu B, Ibáñez M, Valle B, Bilbao J, Gayubo AG, et al. Compositional insights and valorization pathways for carbonaceous material deposited during bio-oil thermal treatment. ChemSusChem 2014;7:2597–608. https://doi.org/10.1002/cssc.201402276.

[43] Meng Y, Contescu CI, Liu P, Wang S, Lee S-H, Guo J, et al. Understanding the local structure of disordered carbons from cellulose and lignin. Wood Sci Technol 2021;55:587–606. https://doi.org/10.1007/s00226-021-01286-6.

[44] Ma Z, Sun Q, Ye J, Yao Q, Zhao C. Study on the thermal degradation behaviors and kinetics of alkali lignin for production of phenolic-rich bio-oil using TGA–FTIR and Py–GC/MS. J Anal Appl Pyrolysis 2016;117:116–24. https://doi.org/10.1016/j.jaap.2015.12.007.

[45] Gu X, Ma X, Li L, Liu C, Cheng K, Li Z. Pyrolysis of poplar wood sawdust by TG-FTIR and Py–GC/MS. J Anal Appl Pyrolysis 2013;102:16–23. https://doi.org/10.1016/j.jaap.2013.04.009.

[46] H. Marsh, F. Rodríguez-Reinoso, Characterization of activated carbon, in: Activated Carbon, Elsevier Science Ltd, 2006: pp. 143–242. https://doi.org/10.1016/B978-008044463-5/50018-2.

[47] Shinde SD, Meng X, Kumar R, Ragauskas AJ. Recent advances in understanding the pseudo-lignin formation in a lignocellulosic biorefinery. Green Chem 2018;20:2192–205. https://doi.org/10.1039/C8GC00353J.

[48] Scholze B, Meier D. Characterization of the water-insoluble fraction from pyrolysis oil (pyrolytic lignin). Part I. PY–GC/MS, FTIR, and functional groups. J Anal Appl Pyrolysis 2001;60:41–54. https://doi.org/10.1016/S0165-2370(00)00110-8.

[49] Gargiulo V, Gomis-Berenguer A, Giudicianni P, Ania CO, Ragucci R, Alfè M. Assessing the potential of biochars prepared by steam-assisted slow pyrolysis for CO_2 adsorption and separation. Energy Fuels 2018;32:10218–27. https://doi.org/10.1021/acs.energyfuels.8b01058.

[50] Fu J, Zhou B, Zhang Z, Wang T, Cheng X, Lin L, et al. One-step rapid pyrolysis activation method to prepare nanostructured activated coke powder. Fuel 2020;262:116514. https://doi.org/10.1016/j.fuel.2019.116514.

[51] N.M. Stark, D.J. Yelle, U.P. Agarwal, Techniques for characterizing lignin, in: O. Faruk, M. Sain (Eds.), Lignin in Polymer Composites, William Andrew, 2016: pp. 49–66. https://doi.org/10.1016/B978-0-323-35565-0.00004-7.

[52] Dissanayake PD, You S, Igalavithana AD, Xia Y, Bhatnagar A, Gupta S, et al. Biochar-based adsorbents for carbon dioxide capture: a critical review. Renew Sust Energ Rev 2020;119:109582. https://doi.org/10.1016/j.rser.2019.109582.

[53] Zhou S, Xue Y, Sharma A, Bai X. Lignin valorization through thermochemical conversion: comparison of hardwood, softwood and herbaceous lignin. ACS Sustain Chem Eng 2016;4:6608–17. https://doi.org/10.1021/acssuschemeng.6b01488.

[54] Domingo-García M, Groszek AJ, López-Garzón FJ, Pérez-Mendoza M. Dynamic adsorption of ammonia on activated carbons measured by flow microcalorimetry. Appl Catal A Gen 2002;233:141–50. https://doi.org/10.1016/S0926-860X(02)00135-7.

[55] Bardestani R, Kaliaguine S. Steam activation and mild air oxidation of vacuum pyrolysis biochar. Biomass Bioenerg 2018;108:101–12. https://doi.org/10.1016/j.biombioe.2017.10.011.

[56] Gasquet V, Kim B, Sigot L, Benbelkacem H. H_2S adsorption from biogas with thermal treatment residues. Waste Biomass Valorization 2020;11:5363–73. https://doi.org/10.1007/s12649-020-00998-3.

[57] Duan C, Ma T, Wang J, Zhou Y. Removal of heavy metals from aqueous solution using carbon-based adsorbents: a review. J Water Process Eng 2020;37:101339. https://doi.org/10.1016/j.jwpe.2020.101339.
[58] Hoang AT, Kumar S, Lichtfouse E, Cheng CK, Varma RS, Senthilkumar N, et al. Remediation of heavy metal polluted waters using activated carbon from lignocellulosic biomass: an update of recent trends. Chemosphere 2022;302:134825. https://doi.org/10.1016/j.chemosphere.2022.134825.
[59] Danish M, Hashim R, Ibrahim MNM, Rafatullah M, Sulaiman O. Surface characterization and comparative adsorption properties of Cr(VI) on pyrolysed adsorbents of *Acacia mangium* wood and *Phoenix dactylifera* L. stone carbon. J Anal Appl Pyrolysis 2012;97:19–28. https://doi.org/10.1016/j.jaap.2012.06.001.
[60] Santhosh KG, Subhani SM, Bahurudeen A. Sustainable reuse of palm oil fuel ash in concrete, alkali-activated binders, soil stabilisation, bricks and adsorbent: a waste to wealth approach. Ind Crops Prod 2022;183:114954. https://doi.org/10.1016/j.indcrop.2022.114954.
[61] Gayathiri M, Pulingam T, Lee KT, Sudesh K. Activated carbon from biomass waste precursors: factors affecting production and adsorption mechanism. Chemosphere 2022;294:133764. https://doi.org/10.1016/j.chemosphere.2022.133764.
[62] Wang B, Gao B, Zimmerman AR, Lee X. Impregnation of multiwall carbon nanotubes in alginate beads dramatically enhances their adsorptive ability to aqueous methylene blue. Chem Eng Res Des 2018;133:235–42. https://doi.org/10.1016/j.cherd.2018.03.026.
[63] Jung K-W, Choi BH, Hwang M-J, Jeong T-U, Ahn K-H. Fabrication of granular activated carbons derived from spent coffee grounds by entrapment in calcium alginate beads for adsorption of acid orange 7 and methylene blue. Bioresour Technol 2016;219:185–95. https://doi.org/10.1016/j.biortech.2016.07.098.
[64] Kazak O, Eker YR, Akin I, Bingol H, Tor A. A novel red mud@sucrose based carbon composite: Preparation, characterization and its adsorption performance toward methylene blue in aqueous solution. J Environ Chem Eng 2017;5:2639–47. https://doi.org/10.1016/j.jece.2017.05.018.
[65] Othman NH, Alias NH, Shahruddin MZ, Abu Bakar NF, Nik Him NR, Lau WJ. Adsorption kinetics of methylene blue dyes onto magnetic graphene oxide. J Environ Chem Eng 2018;6:2803–11. https://doi.org/10.1016/j.jece.2018.04.024.
[66] Liu R-L, Liu Y, Zhou X-Y, Zhang Z-Q, Zhang J, Dang F-Q. Biomass-derived highly porous functional carbon fabricated by using a free-standing template for efficient removal of methylene blue. Bioresour Technol 2014;154:138–47. https://doi.org/10.1016/j.biortech.2013.12.034.
[67] Fan S, Wang Y, Wang Z, Tang J, Tang J, Li X. Removal of methylene blue from aqueous solution by sewage sludge-derived biochar: Adsorption kinetics, equilibrium, thermodynamics and mechanism. J Environ Chem Eng 2017;5:601–11. https://doi.org/10.1016/j.jece.2016.12.019.
[68] Jin Q, Li Y, Yang D, Cui J. Chitosan-derived three-dimensional porous carbon for fast removal of methylene blue from wastewater. RSC Adv 2018;8:1255–64. https://doi.org/10.1039/C7RA11770A.
[69] Wang N, Chen J, Wang J, Feng J, Yan W. Removal of methylene blue by polyaniline/TiO_2 hydrate: adsorption kinetic, isotherm and mechanism studies. Powder Technol 2019;347:93–102. https://doi.org/10.1016/j.powtec.2019.02.049.
[70] Nworie FS, Nwabue FI, Oti W, Mbam E, Nwali BU. Removal of methylene blue from aqueous solution using activated rice husk biochar: adsorption isotherms, kinetics and error analysis. J Chil Chem Soc 2019;64:4365–76. https://doi.org/10.4067/s0717-97072019000104365.
[71] Prajapati AK, Mondal MK. Comprehensive kinetic and mass transfer modeling for methylene blue dye adsorption onto CuO nanoparticles loaded on nanoporous activated carbon prepared from waste coconut shell. J Mol Liq 2020;307:112949. https://doi.org/10.1016/j.molliq.2020.112949.
[72] Salam MA, El-Shishtawy RM, Obaid AY. Synthesis of magnetic multi-walled carbon nanotubes/magnetite/chitin magnetic nanocomposite for the removal of Rose Bengal from real and model solution. J Ind Eng Chem 2014;20:3559–67. https://doi.org/10.1016/j.jiec.2013.12.049.